Yongping Liu ✉
Juan Wang
Changbin Dong
Fuqiang Wang

https://doi.org/10.21278/TOF.491066324
ISSN 1333-1124
eISSN 1849-1391

MATHEMATICAL MODEL AND KINEMATIC CHARACTERISATION OF A NON-CIRCULAR PLANETARY GEAR SYSTEM

Summary

The non-circular gear hydraulic motor is a new type of low-speed and high-torque motor, which is characterised by large unit displacement, smooth operation, high resistance to oil contamination, and high volumetric efficiency. The non-circular planetary gear system, as the core transmission mechanism of the non-circular gear hydraulic motor, and its design accuracy are the key to improving the processing accuracy and transmission performance. Having addressed the issue of designing a non-circular planetary gear system, based on the principle of gear meshing, coordinate transformations and meshing equations of internal and external meshing of the non-circular planetary gear system are solved, a mathematical model of the non-circular planetary gear system is established, and parametric tooth surface equations with a unified expression are obtained. The accuracy of the model is verified through the motion characteristics analysis of the model and the effects of input speed and load on the dynamic meshing characteristics are obtained. The design method proposed in this paper can directly obtain coordinates of the tooth surface data of the sun gear and the ring gear, which is of great significance for improving the efficiency of the dynamic design of the non-circular planetary gear system.

Key words: *non-circular gear, planetary gear system, tooth surface modelling, kinematic analysis*

1. Introduction

The non-circular gear mechanism is widely used in various machines such as multi-joint bionic mechanism [1], continuously variable transmission (CVT) [2], automobiles [3], drainage machines [4] and other kinds of mechanical systems [5-7] due to its characteristic of meeting a specific motion requirement [8]. The non-circular gear planetary drive hydraulic motor is a new type of low-speed and high-torque hydraulic motor, which has the advantages of having a simple structure, small size, light weight, wide speed range and high efficiency [9]. Therefore, it has great application potential and high industrial value.

In 1977, Sieniawski [10] developed the first generation of hydraulic motors using a non-circular planetary gear system as the core mechanism. Over time, non-circular gear hydraulic motors have been more widely used and more demanding requirements on the accuracy of their design were also set. The core mechanism of the non-circular gear hydraulic motor is the non-

circular planetary gear system and the design of a reasonable non-circular planetary gear system is the key to the normal operation of the non-circular gear hydraulic motor.

The tooth profile design of non-circular gears has been extensively investigated by domestic and international researchers. Based on the motion relationship between gears, Li et al. [11] drew the tool profile boundary step by step to get the tooth shape through the extraction of graphic boundaries to come up with a design of the tooth profile of the non-circular planetary gear system. Yv et al. [12] optimised the concave portion of the knuckle curve by using Computer Aided Design (CAD) software, to generate a slave gear tooth profile by applying the principle of the spreading method imitated by the Pro/E software. Ding et al. [13] carried out the parametric modelling of machine tools and tooth fan blanks through secondary development in SolidWorks. Shi et al. [14] generated a tooth profile of the non-circular planetary gear system by using the Unigraphics (UG) software motion simulation and image smoothing technology. Jiang et al. [15] used the tooth profile normal method to generate the tooth profile of non-circular gears for the infinitely variable gear mechanism with high accuracy.

Based on the principle of conjugate meshing, Xin et al. [16] used an approximate numerical algorithm for designing variable-ratio tooth flanks. Litvin et al. [17] used a matrix approach to generate the meshing equations to illustrate the developed theory with an example of elliptical gears. Han et al. [18] proposed a new type of spiral non-bevel gears that can be applied to intersecting shaft variable speed drives using the design principle for non-bevel gears. Liu et al. [19] developed a mathematical model of the noncircular face gear (NFG) generated by a shaper cutter based on the Fourier series method for designing curves. Zheng et al. [20] computed non-circular gears based on the envelope feature using the differential geometry theory and the principle of conjugate tooth profile. Liu et al. [21] used a combination of the commutative tooth shape method and the truncated line to establish a high-order non-circular helical gear model. Han et al. [22] established a linkage model for the hobbing of helical non-cylindrical gears based on the effect of the hob axial feed on the motion of the gear blank. Liu et al. [23] took high-order elliptical gears as the object of study and developed a linkage mathematical model for machining helical non-circular gears by using hobbing cutters. In addition, for the application of double circular pitch curves in non-circular gear hydraulic motors, Xu et al. [24] developed a nonlinear planning model for designing double circular pitch curves. Li et al. [25] proposed a design method for replacing non-circular pitch curves with circular pitch curves of continuously varying curvature.

From the above literature review it can be seen that although researchers have carried out a lot of studies on the design of non-circular gear hydraulic motors, the research methods focused on establishing geometric models of such motors and ignored mathematical models and parametric tooth equations, or they dealt only with a single non-circular gear to parameterise the tooth design and failed to obtain a parameterised tooth model of the non-circular planetary gear system. This resulted in certain limitations on the design of non-circular gear hydraulic motors. Therefore, this paper focuses on the meshing theory of non-circular planetary gear system, establishes a generalised mathematical model of the tooth surface, and verifies the accuracy of the mathematical model and the design method of non-circular planetary gear system through the analysis of motion characteristics.

2. Generation principle of non-circular planetary gear systems

The transmission of the non-circular planetary gear system consists of a sun gear rotating around its own axis, a fixed ring gear, and a sun gear driving the planetary gear to rotate and rotate around the sun gear. The process of generating the non-circular planetary gear system can be regarded as the only rotary motion of the generator and the non-circular gear has both the rotary and the translational motion to ensure that the tangent direction of the pitch circle of the generator and the pitch curve of the non-circular gear is always in the same direction as that of the initial moment.

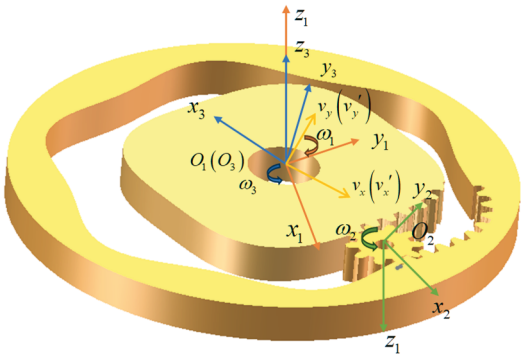

Fig. 1 Generation principle of non-circular planetary gear system

As shown in Fig. 1, the coordinate systems $S_1 - O_1x_1y_1$, $S_2 - O_2x_2y_2$, and $S_3 - O_3x_3y_3$ are established in the sun gear, the generator, and the ring gear, respectively, to describe the generation principle of the non-circular planetary gear system. The generator in the generation process axis is fixed, it rotates around its own axis with angular velocity ω_2. The sun gear and the ring gear rotate along their own axes at angular velocities of ω_1 and ω_3 and move in space at the velocities of v_x, v_y and v_x', v_y', respectively. The tooth profile of the non-circular planetary gear system can be generated by the tooth profile of the generator and all meet the conjugate meshing conditions.

3. Tooth equations for planetary gear systems with non-circular gears

3.1 Tooth surface of the generator

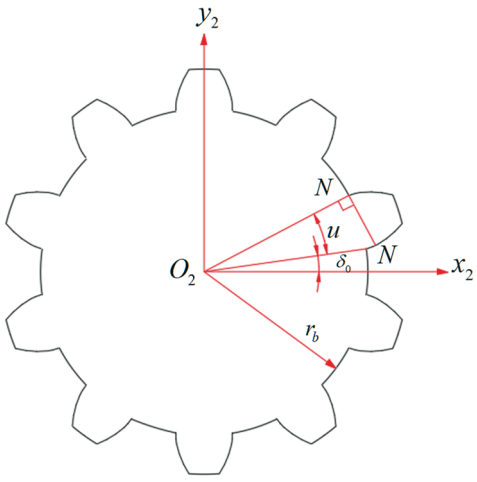

Fig. 2 Involute tooth profile of generator

The non-circular gear with a concave pitch curve cannot be machined by a rack cutter or gear hob. It can only be inserted by a gear shaper cutter with a proper diameter. The non-circular planetary gear system with a concave pitch curve is a relatively common phenomenon. Therefore, the method for solving the tooth surface equation of the non-circular planetary gear system established in this paper is based on the principle of gear shaping and the tooth surface equation of the non-circular gear is obtained by the tooth surface equation of the generator.

Fig. 2 shows the involute tooth profile of a single generator. During the process of machining the non-circular gear, the generator moves in its axial direction and the tooth surface of the generator is expressed as:

$$r_s = \begin{bmatrix} x_s \\ y_s \\ z_s \\ t_s \end{bmatrix} = \begin{bmatrix} r_b[\cos(\delta_0 + u_s) + u_s \sin(\delta_0 + u_s)] \\ r_b[\sin(\delta_0 + u_s) - u_s \sin(\delta_0 + u_s)] \\ v_s \\ 1 \end{bmatrix} \tag{1}$$

where, r_b is the radius of the base circle of the generator, μ_s is the involute spreading angle, δ_0 is the half angle of the base circle tooth groove, v_s is the movement speed of the generator.

The normal vector n_s at any point on the generator is expressed as:

$$n_s = \frac{\partial r_s}{\partial u_s} \times \frac{\partial r_s}{\partial v_s} \tag{2}$$

The expression for the normal vector of the generator can be expressed as:

$$\begin{cases} n_x = r_b u_s \sin(\delta_0 + u_s) \\ n_y = -r_b u_s \cos(\delta_0 + u_s) \\ n_{z=0} \end{cases} \tag{3}$$

3.2 Pitch curve of the non-circular planetary gear system

In the non-circular planetary gear system, the pitch curve of the sun gear is a high-order elliptical gear and its pitch curve equation is expressed as:

$$\begin{cases} r_1 = \dfrac{p}{1 + k\cos(n_1\theta_1)} \\ p = A(1 - k^2) \end{cases} \tag{4}$$

where k is the eccentricity, n_1 is the order, θ_1 is the polar angle, and A is the radius of the long axis.

The closing condition of the pitch curve of the sun gear and the ring gear is expressed as:

$$\frac{2\pi}{n_3} = \int_0^{\frac{2\pi}{n_1}} \frac{r_1}{r_3} \mathrm{d}\theta_1 + \int_0^{\frac{2\pi}{n_1}} \frac{2r_2 \sin\mu_1}{r_3} \mathrm{d}\theta_1 \tag{5}$$

where r_2 and r_3 denote the radii of the planetary gear and the ring gear, respectively, and n_3 denotes the order of the ring gear. In order to describe the tangent direction of the pitch curve of the non-circular gear and the generator, μ_1 is defined as the angle formed by the radial diameter between the tangent and the non-circular gear, which can be determined by the following equation:

$$\tan\mu_1 = \frac{r_1(\varphi_1)}{\dfrac{\mathrm{d}r_1(\varphi_1)}{\mathrm{d}\varphi_1}} \tag{6}$$

Furthermore, to ensure that all gear teeth are uniformly spaced along the pitch curve and that each gear has the same modulus, the number of teeth and the modulus should satisfy the following equation:

$$\pi mz = L = \int_0^{2\pi} \sqrt{r_1(\varphi_1)^2 + \left(\frac{\mathrm{d}r_1(\varphi_1)}{\mathrm{d}\varphi_1}\right)^2}\,\mathrm{d}\varphi_1 \tag{7}$$

where L is the arch length of the pitch curve and φ_1 is the rotation angle of the sun gear.

According to the basic kinematic relationship of non-circular planetary gears, the equation of the pitch curve of the ring gear is expressed as:

$$\begin{cases} r_3 = r_1 + 2r_2 \sin\mu_1 \\ \theta_3 = \int_0^{\theta_1} \dfrac{r_1}{r_3}\mathrm{d}\theta_1 + \int_0^{\theta_1} \dfrac{2r_3 \sin\mu_1}{r_3}\left(\dfrac{\mathrm{d}\mu_1}{\mathrm{d}\theta_1}\right)\mathrm{d}\theta_1 \end{cases} \tag{8}$$

The condition that the non-circular planetary gear system does not produce motion interf erence during operation is expressed as:

$$r_{3\min} \geq r_{1\max} + 2h_a \tag{9}$$

By using the above equations, the pitch curve of the non-circular planetary gear system is obtained as shown in Fig. 3.

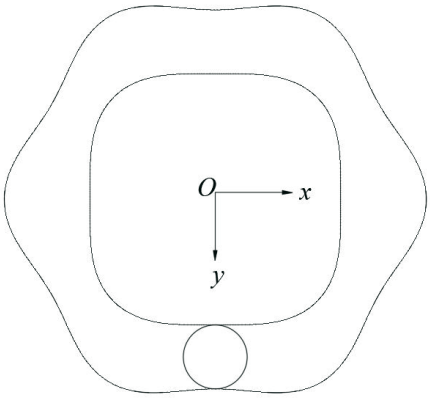

Fig. 3 Pitch curve of non-circular planetary gear system

3.3 Relative motion and coordinate systems

In order to clearly describe the coordinate transformation relationship between the generator and the non-circular gears, several coordinate systems are established, as shown in Fig. 4.

In the relative motion of the sun gear and the generator, $S_f(x_f - y_f - z_f)$ is a coordinate fixed in space and $S_s(x_s - y_s - z_s)$ is fixed at the centre of the generator. Coordinate $S_m(x_m - y_m - z_m)$ is used to describe the translational motion of the sun gear, x_m is the axis parallel to the x_f axis, the y_m axis is parallel to the y_f axis in the opposite direction, and the z_m axis is parallel to the z_f axis. $S_p(x_p - y_p - z_p)$ is fixed to the centre of the sun gear and z_p the sun gear rotates around.

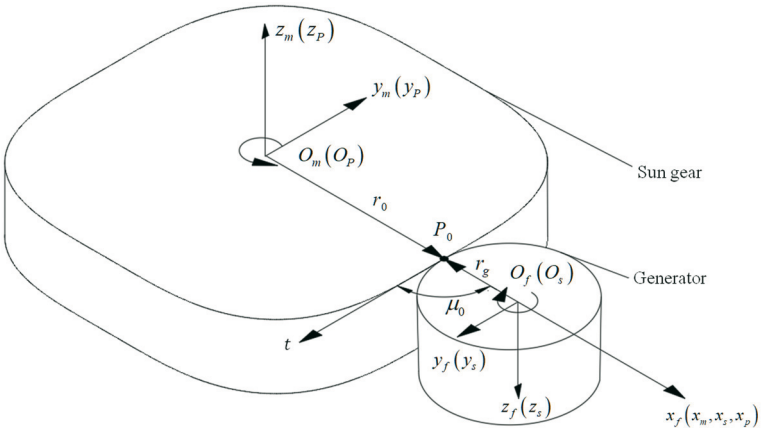

Fig. 4 Coordinate system of sun gear and generator

Similarly, the coordinate systems $S_f'(x_f' - y_f' - z_f')$, $S_s'(x_s' - y_s' - z_s')$, $S_m'(x_m' - y_m' - z_m')$ and $S_p'(x_p' - y_p' - z_p')$ are established to describe the motion of the ring gear.

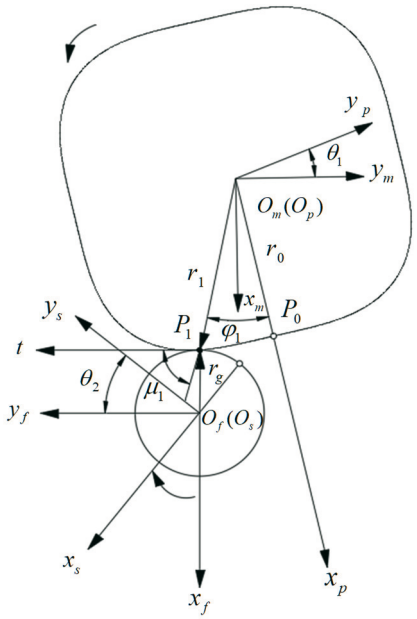

Fig. 5 Coordinate transformation of sun gear and generator

In Fig. 5, the angle of rotation of the sun gear is θ_1 , the polar angle is φ_1 , the radial diameter is r_1 , and the tangent point is $P_1(r_1, \varphi_1)$. The centre of rotation of the sun gear can be determined by the following equation:

$$\begin{cases} x = -\left(r_1 \sin \mu_1 + r_g\right) \\ y = r_1 \cos \mu_1 \end{cases} \tag{10}$$

where r_g is the radius of the pitch circle of the generator, and $\mu_1 = \arctan\left(\dfrac{r_1(\varphi_1)}{\dfrac{\mathrm{d}r_1(\varphi_1)}{\mathrm{d}\varphi_1}}\right)$

The arc length of the sun gear pitch curve can be calculated as:

$$L_1 = \int_{\varphi_0}^{\varphi_1} \sqrt{r(\varphi_1)^2 + \left(\frac{\mathrm{d}r(\varphi_1)}{\mathrm{d}\varphi_1}\right)^2}\,\mathrm{d}\varphi_1 \tag{11}$$

Then, the angular displacements θ_1 and θ_2 of the sun gear and the generator can be expressed as:

$$\begin{cases} \theta_1 = \varphi_1 - \varphi_0 - \mu_0 + \mu_1 \\ \theta_2 = \dfrac{L_1}{r_g} \end{cases} \tag{12}$$

Similarly, the arc length of pitch curve and the angular displacement of the ring gear can be expressed as:

$$L_3 = \int_{\varphi_0}^{\varphi_3} \sqrt{r(\varphi_3)^2 + \left(\frac{\mathrm{d}r(\varphi_3)}{\mathrm{d}\varphi_3}\right)^2}\,\mathrm{d}\varphi_3 \tag{13}$$

$$\begin{cases} \theta_3 = \varphi_3 - \varphi_0 - \mu_0 + \mu_3 \\ \theta_2 = \dfrac{L_3}{r_g} \end{cases} \tag{14}$$

The relationship between the coordinate transformation of the generator and the sun gear is as follows:

The transformation relationship from S_m to S_p can be written as:

$$\begin{bmatrix} x_p \\ y_p \\ z_p \\ t_p \end{bmatrix} = M_{pm} \begin{bmatrix} x_m \\ y_m \\ z_m \\ t_m \end{bmatrix} \quad M_{pm} = \begin{bmatrix} \cos\theta_1 & \sin\theta_1 & 0 & 0 \\ -\sin\theta_1 & \cos\theta_1 & 0 & 0 \\ 0 & 0 & 1 & 0 \\ 0 & 0 & 0 & 1 \end{bmatrix} \tag{15}$$

The transformation relationship from S_f to S_m can be written as:

$$\begin{bmatrix} x_m \\ y_m \\ z_m \\ t_m \end{bmatrix} = M_{mf} \begin{bmatrix} x_f \\ y_f \\ z_f \\ t_f \end{bmatrix} \quad M_{mf} = \begin{bmatrix} 1 & 0 & 0 & r_g + r_1 \sin(\mu_1) \\ 0 & -1 & 0 & -r_1 \cos(\mu_1) \\ 0 & 0 & -1 & 0 \\ 0 & 0 & 0 & 1 \end{bmatrix} \tag{16}$$

The transformation relationship from S_s to S_f can be written as:

$$\begin{bmatrix} x_f \\ y_f \\ z_f \\ t_f \end{bmatrix} = M_{fs} \begin{bmatrix} x_s \\ y_s \\ z_s \\ t_s \end{bmatrix} \quad M_{fs} = \begin{bmatrix} \cos\theta_2 & -\sin\theta_2 & 0 & 0 \\ \sin\theta_2 & \cos\theta_2 & 0 & 0 \\ 0 & 0 & 1 & 0 \\ 0 & 0 & 0 & 1 \end{bmatrix} \tag{17}$$

The coordinate transformation from the generator to the ring gear is as follows:

The transformation relationship from S_m' to S_P' can be written as:

$$\begin{bmatrix} x_p' \\ y_p' \\ z_p' \\ t_p' \end{bmatrix} = M_{pm}' \begin{bmatrix} x_m' \\ y_m' \\ z_m' \\ t_m' \end{bmatrix} \quad M_{pm}' = \begin{bmatrix} \cos\theta_1 & \sin\theta_1 & 0 & 0 \\ -\sin\theta_1 & \cos\theta_1 & 0 & 0 \\ 0 & 0 & 1 & 0 \\ 0 & 0 & 0 & 1 \end{bmatrix} \tag{18}$$

The transformation relationship from S_f' to S_m' can be written as:

$$\begin{bmatrix} x_m' \\ y_m' \\ z_m' \\ t_m' \end{bmatrix} = M_{mf}' \begin{bmatrix} x_f' \\ y_f' \\ z_f' \\ t_f' \end{bmatrix} \quad M_{mf}' = \begin{bmatrix} 1 & 0 & 0 & r_g - r_1\sin(\mu_1) \\ 0 & -1 & 0 & -r_1\cos(\mu_1) \\ 0 & 0 & -1 & 0 \\ 0 & 0 & 0 & 1 \end{bmatrix} \tag{19}$$

The transformation relationship from S_s' to S_f' can be written as:

$$\begin{bmatrix} x_f' \\ y_f' \\ z_f' \\ t_f' \end{bmatrix} = M_{fs}' \begin{bmatrix} x_s' \\ y_s' \\ z_s' \\ t_s' \end{bmatrix} \quad M_{fs}' = \begin{bmatrix} -\cos\theta_2 & \sin\theta_2 & 0 & 0 \\ \sin\theta_2 & \cos\theta_2 & 0 & 0 \\ 0 & 0 & 1 & 0 \\ 0 & 0 & 0 & 1 \end{bmatrix} \tag{20}$$

3.4 Meshing equation

A pair of conjugate tooth flanks, whether made in point or line contact, must satisfy the meshing equation at the point of contact, which is usually expressed as:

$$n_s \cdot v_{sp} = 0 \tag{21}$$

where n_s is the normal vector of the generator teeth and v_{sp} is the relative velocity between the conjugate tooth surfaces.

The above meshing equation can be solved for the angle of rotation of the gear corresponding to a contact point on the tooth surface. In the process of generating the non-circular gear by the generator, the position of the coordinate system S_f fixed in space is always kept constant, and the pitch circle of the generator is always kept in the tangent relationship with the pitch curve of the non-circular gear. The rotation angle of the generator and the parameter of the tooth surface can be linked by the meshing equation, so as to obtain the equation of the tooth surface of the non-circular gear.

According to the principle of gear meshing, the external meshing equation for parallel shaft internal and external cylindrical gearing can be expressed as:

$$\begin{cases} U\cos\theta_2 - V\sin\theta_2 = W \\ U = i_{21}an_y^{(s)} \\ V = -i_{21}an_x^{(s)} \\ W = \left(1+i_{21}\right)\left(y_s n_x^{(s)} - x_s n_y^{(s)}\right) \end{cases} \tag{22}$$

The internal meshing equation can be expressed as:

$$\begin{cases} U\cos\theta_2 - V\sin\theta_2 = W \\ U = -i_{21}an_y^{(s)} \\ V = i_{21}an_x^{(s)} \\ W = \left(1-i_{21}\right)\left(y_s n_x^{(s)} - x_s n_y^{(s)}\right) \end{cases} \tag{23}$$

where $n_x^{(s)}$ and $n_y^{(s)}$ are the projections of the normal vector n_s on the axes x_s and y_s of the coordinate system S_s.

The final meshing equation for both internal and external meshing simplifications are obtained as:

$$\theta_2 = \pm\arccos\left(-\frac{r_b}{r_g}\right) \pm \left(\delta_0 + u_s + v_s\right) \tag{24}$$

The coordinates S_s fixed in the generator are transformed into the coordinates S_p of the sun gear and the coordinates S_p' of the ring gear. Then, the equation of the tooth surface of the non-circular planetary gear system is shown in Eq. (25), in which the upper and lower symbols $\pm$ denote the left-hand and right-hand sides of the tooth surface, respectively.

$$\begin{cases} \sum p = M_{pm}\left(\theta_i\right) M_{mf}\left(r_i, \mu_i\right) M_{fs}\left(\phi_i\right) r_s\left(u_s, v_s\right) \\ \sum p' = M_{pm}'\left(\theta_i\right)' M_{mf}'\left(r_i, \mu_i\right)' M_{fs}'\left(\phi_i\right)' r_s\left(u_s, v_s\right) \\ \theta_2 = \pm\arccos\left(-\frac{r_b}{r_g}\right) \pm \left(\delta_0 + u_s + v_s\right) \end{cases} \tag{25}$$

4. Geometric design and kinematic analysis

4.1 Model building and motion analysis

Taking the gear parameters shown in Table 1 as an example, the tooth data obtained by solving the tooth equations are shown in Fig. 6. The parameters of the non-circular planetary gear system are shown in Table 1.

Table 1 Parameters of the non-circular planetary gear system

Parameter	Sun gear	Ring gear
Pitch curve order	4	6
Number of teeth	44	66
Modulus (mm)	2	2
Tooth width (mm)	10	10
Addendum coefficient	0.8	0.8
Tip clearance coefficient	0.12	0.12

A model of the non-circular planetary gear system is obtained through 3D software processing as shown in Fig. 7:

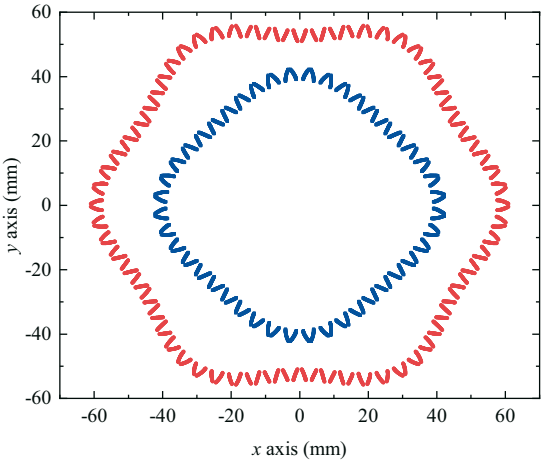

Fig. 6 Non-circular gear tooth surface coordinates

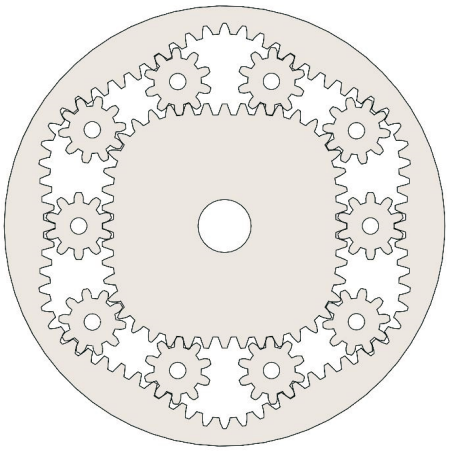

Fig. 7 Non-circular planetary gear system model

4.2 Dynamic characteristics analysis

In the virtual prototype simulation software, according to the Hertz collision theory, the normal contact force in the collision function is defined as:

$$F_n = \begin{cases} K\delta^n + \text{step}\left(\delta, 0, \delta_{\max}, C_{\max}\right)\dfrac{\mathrm{d}\delta}{\mathrm{d}t}, \delta \geq 0 \\ 0, \delta < 0 \end{cases} \tag{26}$$

where K is the gear contact stiffness coefficient, δ is the deformation of the gear meshing point during collision, i is the collision coefficient, $\delta_{\max}$ is the maximum deformation, t is the time of collision deformation, $\text{step}()$ is a step function, and $C_{\max}$ is the maximum damping coefficient.

The contact stiffness coefficient K can be replaced by the contact stiffness in the Hertz static elastic contact theory. It can be expressed as:

$$K = \frac{4}{3}\rho^{\frac{1}{2}}E \tag{27}$$

In the formula, ρ is the comprehensive curvature radius, which can be expressed as:

$$\frac{1}{\rho} = \frac{1}{\rho_1} + \frac{1}{\rho_2} \tag{28}$$

where ρ_1 and ρ_2 are the equivalent radii of the contact point. The comprehensive radius of the curvature of the non-circular gear can be expressed as:

$$\rho^*(\varphi) = P\frac{[(1-k\cos n\varphi)^2 + k^2n^2\sin^2 n\varphi]^{3/2}}{(1-k\cos n\varphi)^3[(1+k(n^2-1)\cos n\varphi)} \tag{29}$$

$$P = A(1-k^2) \tag{30}$$

E is the comprehensive elastic modulus, which can be expressed as:

$$\frac{1}{E} = \frac{1-\mu_1^2}{E_1} + \frac{1-\mu_2^2}{E_2} \tag{31}$$

where E_1 and E_2 are the elastic moduli of the gear material.

The gear material selected in this paper is structural steel with the following properties: elastic modulus $E = 2.1\times10^9$ Pa, Poisson's ratio $\mu_1 = \mu_2 = 0.3$, collision coefficient $i = 1$, deformation of the gear meshing point $\delta = 0.1$ mm, and the maximum damping coefficient is 1% of the stiffness.

Based on the virtual prototype model, the constraints and loads added to the system are as follows. A revolute joint is applied to the sun gear, and a fixed joint is applied to the ring gear. The solid-solid contact is applied to the gear train to simulate the gear meshing transmission. A constant speed drive is applied at the revolute joint of the sun gear. Different loads are applied to the planetary gear to simulate the working load of the gear train. The rotation speed of the sun gear is set to 120 deg/s. The simulation time is 10 s, and the number of simulation steps is set to 5,000 steps.

The angular displacement and angular velocity curves of the sun gear and planetary gear are analysed, as shown in Figs. 8 and 9, and the kinematic characteristics of the planetary gear show obvious periodic changes. According to the basic kinematic relationship, there exists a relational equation between the planetary gear angular velocity ω_2 and the sun gear angular velocity ω_1 [14]:

$$\frac{\omega_2}{\omega_1} = \frac{r_1\cos\alpha_1}{r_2\cos\alpha'} \tag{32}$$

The angular displacement and angular velocity curves of the sun gear and planetary gears are compared with Eq. (26), and the trends are consistent with the theoretical analysis. In addition, the accuracy of the generation method and the generated mathematical model is demonstrated.

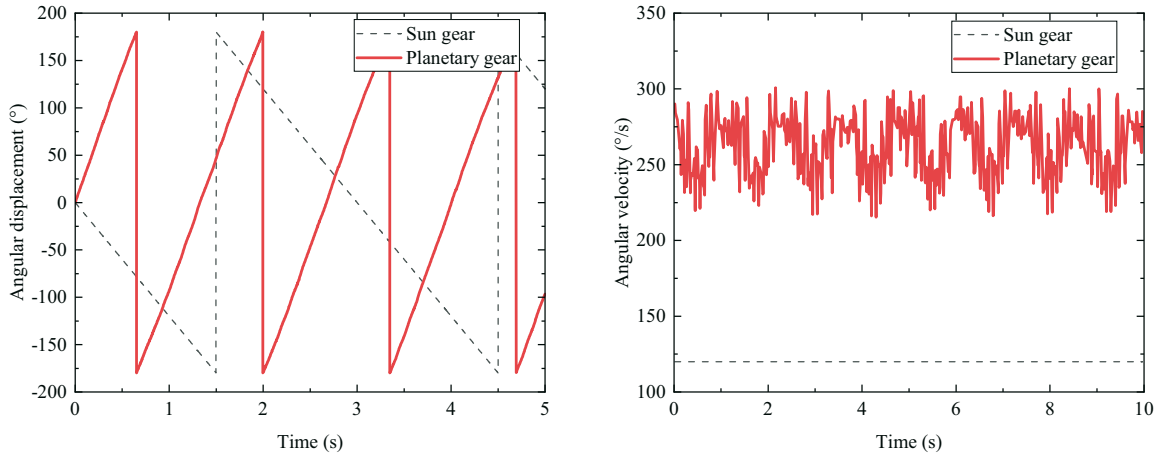

(*a*) Angular displacement (*b*) Angular velocity

Fig. 8 Angular displacement and angular velocity curves of sun gear and planetary gear

4.3 Effect of different input speeds on the dynamic meshing characteristics of gears under no load

Under no-load conditions, the rotational speeds of 100 deg/s, 150 deg/s and 200 deg/s were applied to the sun gear to investigate the changes in the dynamic meshing characteristics of the gear teeth under no load. As can be seen from Fig. 9, the radial, tangential and total displacement images of the planetary gear at different rotational speeds under no-load conditions are all cyclic and as the rotational speeds increase, the radial and tangential displacement periods become shorter.

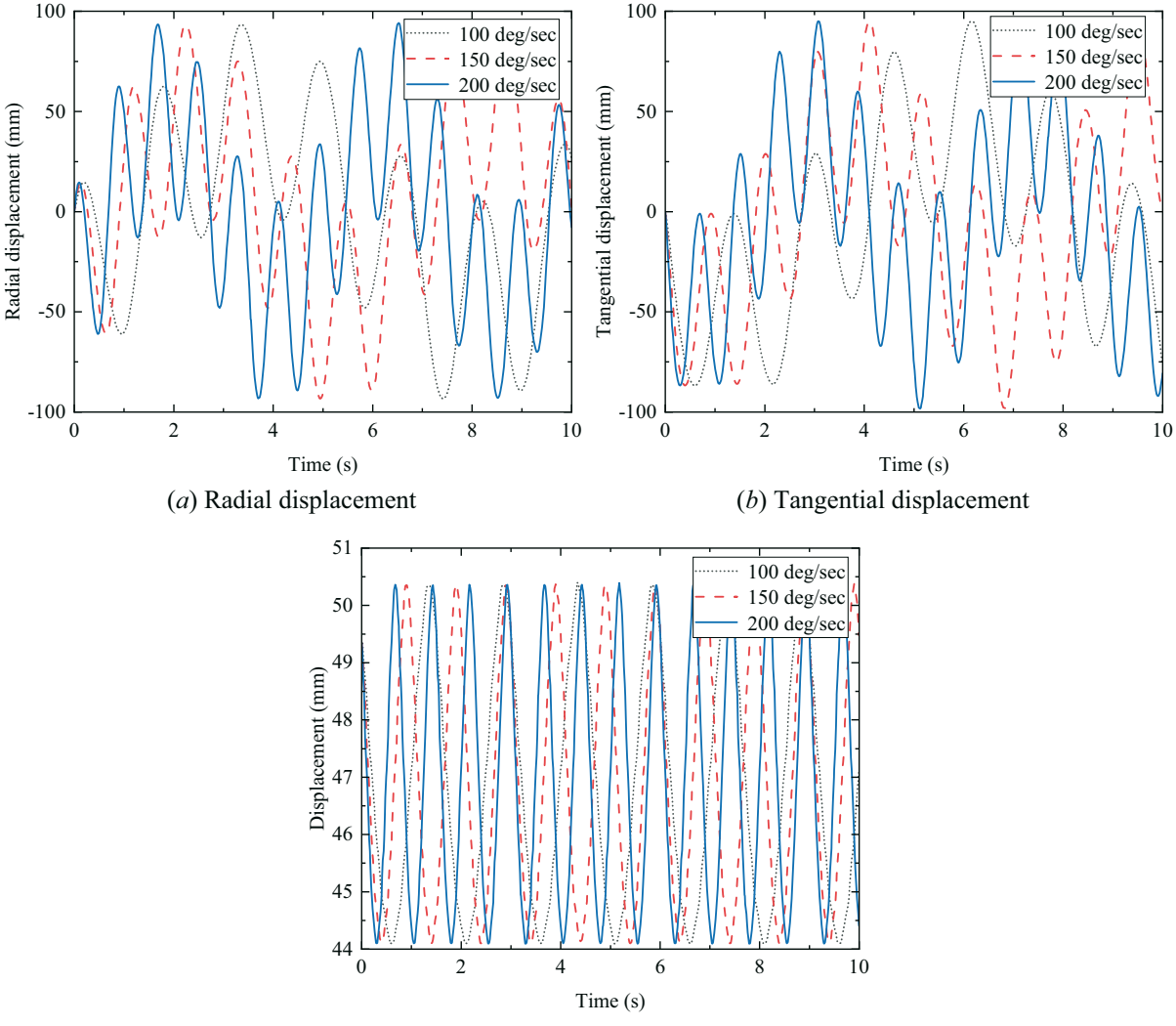

(*a*) Radial displacement (*b*) Tangential displacement

(*c*) Displacement

Fig. 9 Radial, tangential and total displacements of planetary gear at different speeds under no load

The force on the contact of the two pairs of gears of the sun gear and the planetary gear and the planetary gear and the ring gear are analysed. As can be seen from Fig. 10, with an increase in the rotational speed, the dynamic engagement force between the gear teeth is consistent with the change trend of the torque. After entering the meshing period, the engagement force of the gear is sinusoidal and has obvious periodicity.

From Figs. 10 and 11, it can be seen that in the transmission process the position of the maximum force on the gear teeth of the non-circular planetary gear system occurs at the maximum pole diameter of the sun gear and the ring gear. The maximum position of the force appears in the third peak; this is because, when the planetary gear is in the maximum position of the pole diameter of the sun gear of the driving torque and the gravity of the combined torque

is the largest and with an increase in the input speed, the overall amplitude of the engagement force increases and the cycle becomes shorter. The impact vibration between the gear teeth meshing-in and meshing-out increases, resulting in increased wear between the gear teeth and reducing the service life of the gear teeth. Thus, in practice, the rotational speed should not be too large. The engagement force and the torque of the gear contact between the planetary gear and the ring gear are consistent with the law of the sun gear and the planetary gear.

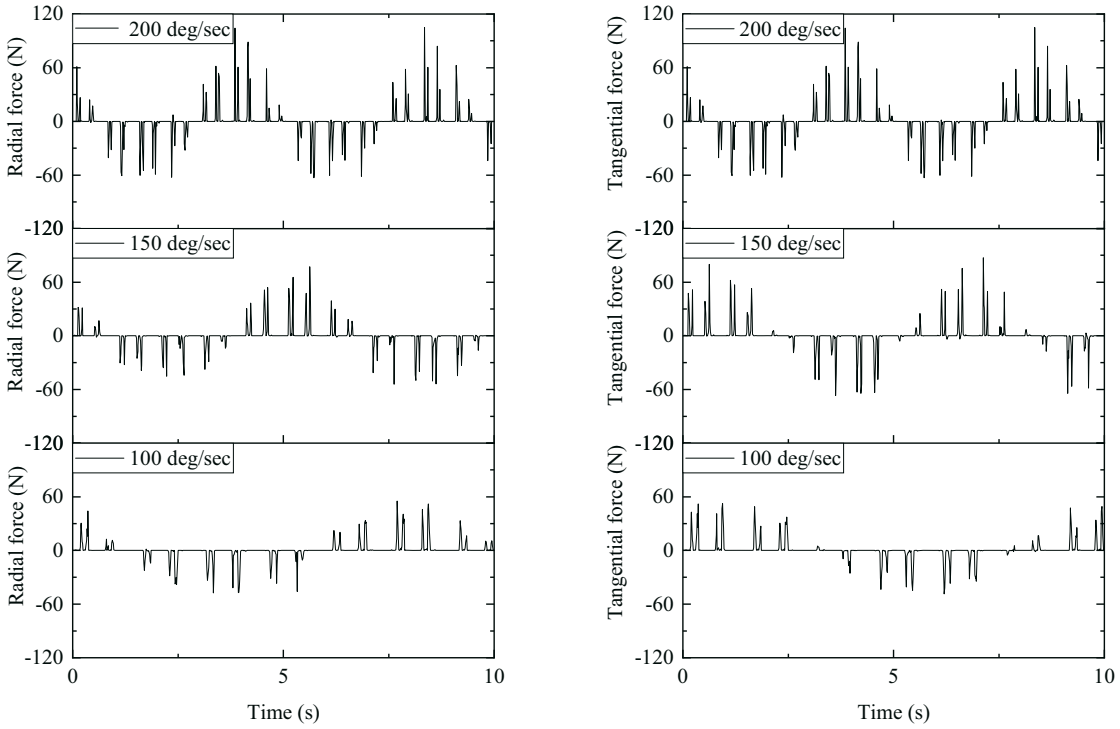

(*a*) Radial engagement force (*b*) Tangential engagement force

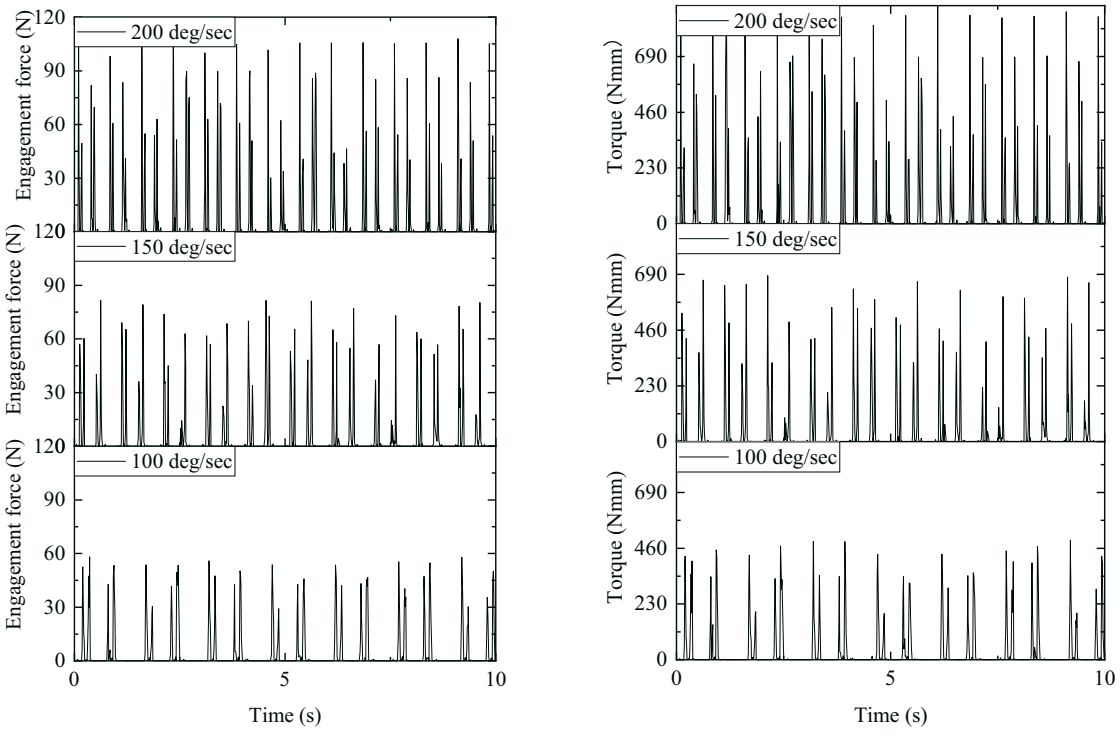

(*c*) Engagement force (*d*) Torque

Fig. 10 Time-domain plots of variation of engagement force and torque of planetary gear by sun gear at different rotational speeds under no load

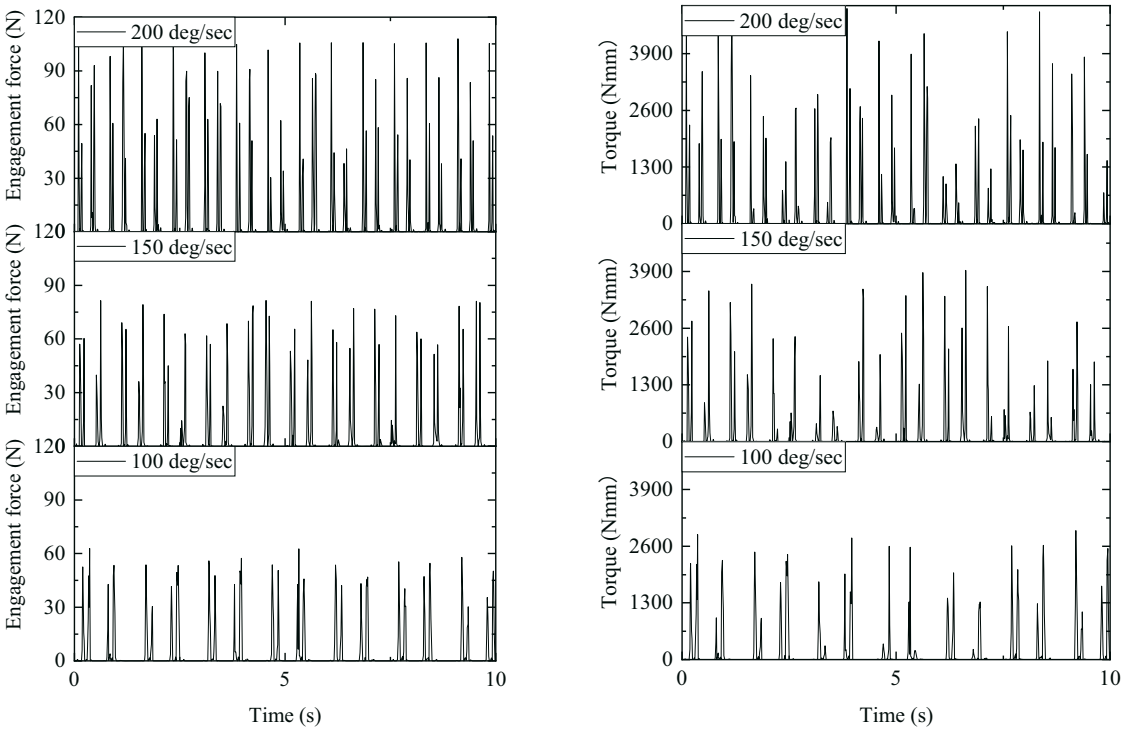

(*a*) Engagement force (*b*) Torque

Fig. 11 Time-domain plots of variation of engagement force and torque of planetary gear by ring gear at different rotational speeds under no load

Fig. 12 shows a frequency domain diagram of the change of engagement force of the planetary gear subjected to the sun gear under different rotational speed conditions. The frequencies of the engagement force between the gear teeth are different. With an increase in the rotational speed, the fluctuation range of the engagement force shows an increasing trend and the fluctuation of the frequency of the engagement force reflects the smoothness of the gear tooth transmission. So it can be seen that, with an increase in the rotational speed of the gear teeth in the transmission of the process of meshing-in and meshing-out the impact increases and the frequency of vibration is elevated, increasing the degree of wear and tear of the tooth contact and affecting the service life of the gears.

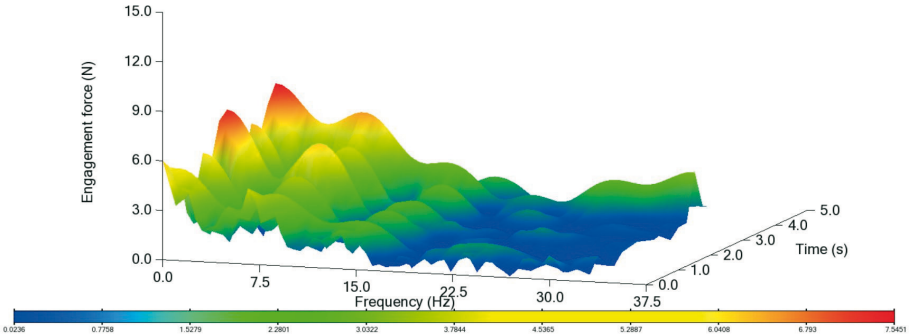

(*a*) Frequency domain diagram of engagement force change when speed of sun gear is 100 deg/s

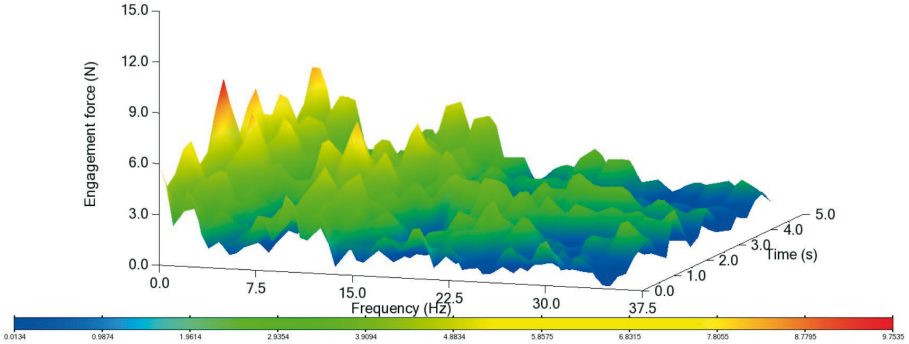

(*b*) Frequency domain diagram of engagement force change when speed of sun gear is 150 deg/s

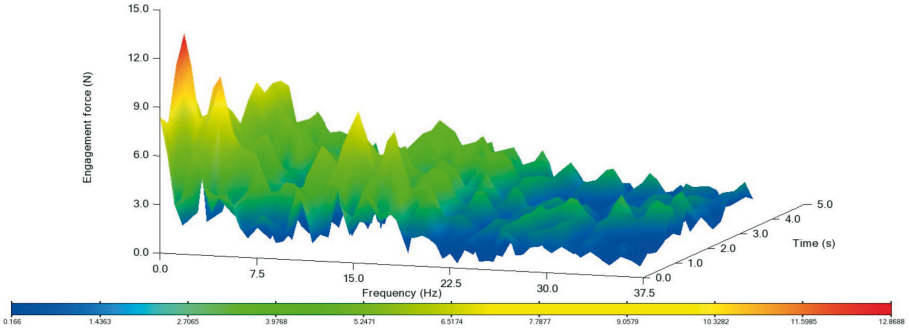

(*c*) Frequency domain diagram of engagement force change when speed of sun gear is 200 deg/s

Fig. 12 Frequency domain diagram of variation of engagement force of planetary gear by sun gear at different rotational speeds under no load

4.4 Effect of different constant loads on the dynamic meshing characteristics of gears

Figs. 13 and 14 show the amplitude variation curves of the engagement force and torque of the planetary gear subjected to the sun gear and ring gear under different constant loads. When the rotational speed is constant, the dynamic engagement force between the gear teeth increases with an increase in the load acting on the planetary gear. The reason for this phenomenon is that during the meshing process of the gear teeth, the contact deformation between the gear teeth increases with an increase in the load torque, which ultimately leads to a proportional increase in the engagement force between the gear teeth of the non-circular planetary gear system.

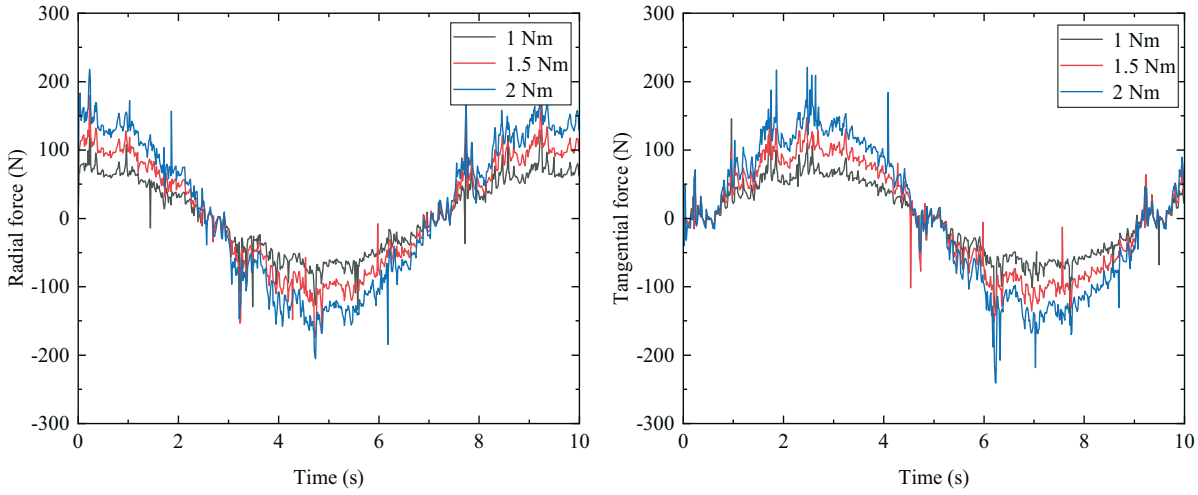

(*a*) Radial engagement force

(*b*) Tangential engagement force

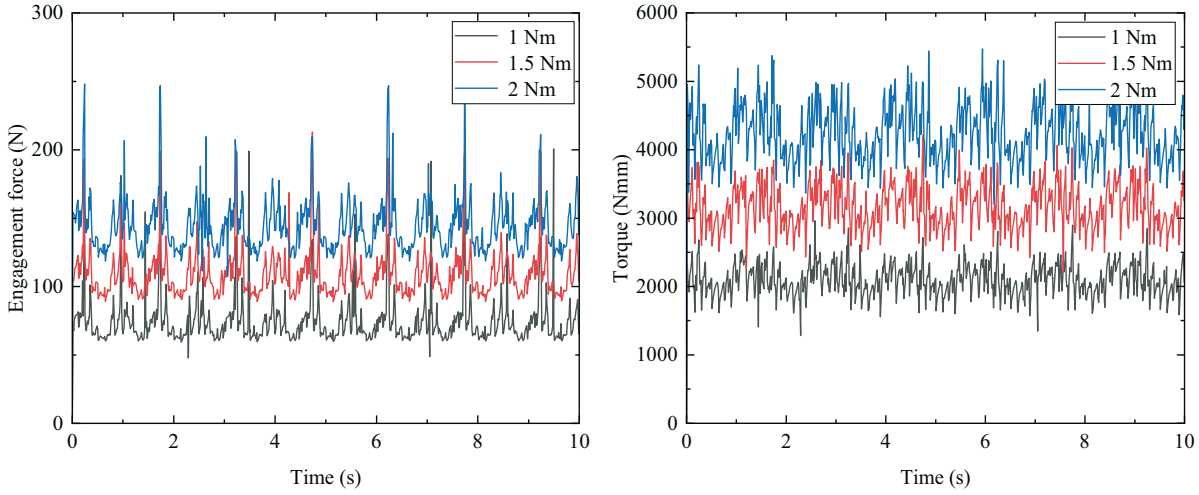

(c) Engagement force (*d*) Torque

Fig. 13 Engagement force and torque of planetary gear by sun gear under different constant loads

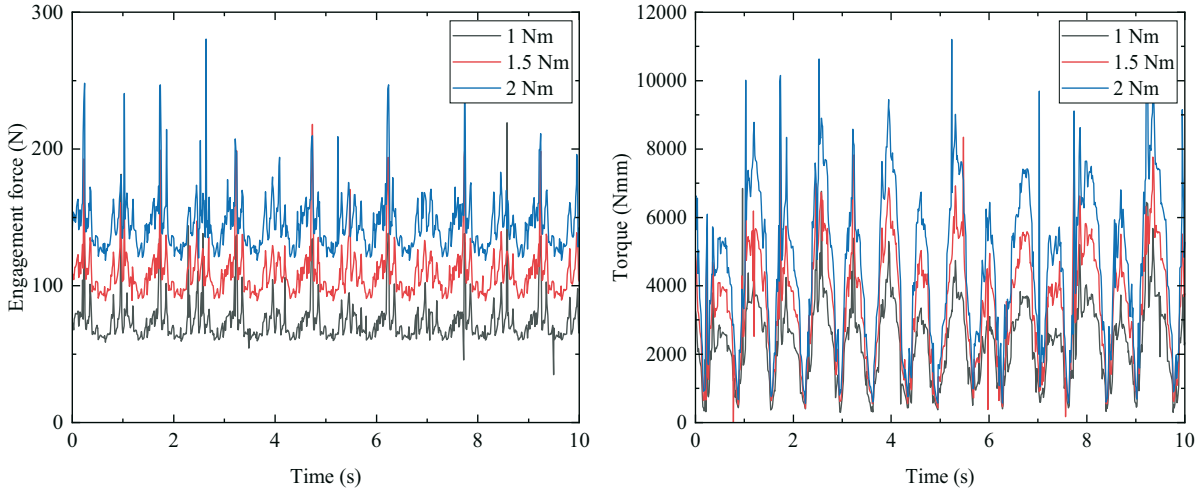

(*a*) Engagement force (*b*) Torque

Fig. 14 Engagement force and torque of planetary gears by ring gear under different constant loads

5. Conclusions

In this paper, based on the theory of gear meshing, the tooth surface equations of the non-circular planetary gear system are investigated with the aim of establishing a mathematical model of the tooth surface to compensate for the design defects of the non-circular planetary gear system and of providing a basis for the study of the dynamics characteristics of the non-circular planetary gear system. The following conclusions can be drawn:

(1) A general tooth surface equation of the parametric non-circular planetary gear system is obtained, by which the coordinate values of the points on the tooth surface of the non-circular planetary gear system can be obtained directly.

(2) The calculation results show that the kinematic performance of the non-circular planetary gear system obtained by this method is consistent with the theoretical value, which verifies the accuracy of the model.

(3) Through the dynamic analysis of the non-circular planetary gear system, the dynamic meshing characteristics of the planetary gear system under different working

conditions are obtained, which provides a reference basis for the application of the non-circular planetary gear system.

(4) The main future work will focus on the contact characteristics of the non-circular planetary gear system and on the non-circular gear design methods that take modification into account.

Acknowledgement

This study was sponsored by the National Natural Science Foundation of China (No. 52265008), the Gansu Province Youth Science Foundation Project of China (23JRRA751), the Gansu Provincial Department of Education of China: Innovation Fund Project for University Teachers (2023A-021), and the Wenzhou Municipal Basic Scientific Research Project (2022G0145).

REFERENCES

[1] Liu, D.; Zhang, T.; Cao, Y. Multi-Joint Bionic Mechanism Based on Non-Circular Gear Drive. *Biomimetics* **2023**, *8*, 272. https://doi.org/10.3390/biomimetics8030272

[2] Li, G.; Zhu, W. Design and power loss evaluation of a noncircular gear pair for an infinitely variable transmission. *Mechanism and Machine Theory* **2021**, *156*. https://doi.org/10.1016/j.mechmachtheory.2020.104137

[3] Ding, G.; Wu, X.; Li, T.; Liu, H.; Zhou, M; Yu, J. Research on the varying-displacement-coefficient modification method for automobile steering noncircular sector gears. *Mechanism and Machine Theory* **2022**, *176*. https://doi.org/10.1016/j.mechmachtheory.2022.105008

[4] Xu, G.; Hua, D.; Dai, W.; Zhang, X. Design and Performance Analysis of a Coal Bed Gas Drainage Machine Based on Incomplete Non-Circular Gears. *Energies* **2017**, *10*, 1933. https://doi.org/10.3390/en10121933

[5] Suh, J.; Kim, K. Harmonious Cable Actuation Mechanism for Soft Robot Joints Using a Pair of Noncircular Pulleys. *Journal of Mechanisms and Robotics* **2018**, *10*, 061002. https://doi.org/10.1115/1.4041055

[6] Zhang, B.; Song, S.; Jing, C.; Xiang D. Displacement prediction and optimization of a non-circular planetary gear hydraulic motor. *Advances in Mechanical Engineering* **2021**, 13. https://doi.org/10.1177/16878140211062690

[7] Xu, G.; Chen, J.; Zhao, H. Numerical Calculation and Experiment of Coupled Dynamics of the Differential Velocity Vane Pump Driven by the Hybrid Higher-order Fourier Non-circular Gears. *Journal of Thermal Science* **2018**, *27*, 285-293. https://doi.org/10.1007/s11630-018-1010-7

[8] Dong, C.; Li, L.; Liu, Y; Wei, Y. Translation torsion coupling dynamic modeling and nonlinearities investigation of non-circular planetary gear systems. *Nonlinear Dyn* **2024**. https://doi.org/10.1007/s11071-024-10004-3

[9] Dong, C.; Liu, Y. Experimental study on transmission error and dynamic backlash of elliptic gear transmission system. *Proceedings of the Institution of Mechanical Engineers, Part K: Journal of Multi-body Dynamics* **2022**, *236*, 130-139. https://doi.org/10.1177/14644193221077494

[10] Sieniawski, B. Gyrating-cam engine, particularly as a hydraulic engine. *U.S. Patent* **1974**, *3*, 852.

[11] Li, J.; Wu, X.; Mao, S. Numerical computing method of noncircular gear tooth profiles generated by shaper cutters. *The International Journal of Advanced Manufacturing Technology* **2007**, *33*, 1098-1105. https://doi.org/10.1007/s00170-006-0560-0

[12] Yu, G.; Yu, J.; Tong, J.; Ye, C.; Zheng, S. Design of a Conjugate Concave-Convex Non–circular Gear Mechanism. *China Mechanical Engineering* **2016**, *27*, 2155-2159+2165.

[13] Ding, G.; Shen, G.; Zhou, H.; Zhou, G. Three-dimensional parametric modeling of non-circular gear sector of automobile steering arm. *Mechanical Science and Technology for Aerospace Engineering* **2020**, *39*, 1242-1247. https://doi.org/10.13433/j.cnki.1003-8728.20190207

[14] Shi, N.; Liu, Q.; Li, Q.; Li, K. 3D parametric modeling of non-circular planetary gear hydraulic motors. *Journal of Ordnance Equipment Engineering* **2023**, *44*, 234-240.

[15] Jiang, C.; Qiu, W.; Li, S.; Zhao, C.; Zhan, J. Precise Design of Non-circular Gear of a Infinitely Variable Transmission. *Mechanical & Electrical Engineering Technology* **2021**, *50*, 225-231.

[16] Xin, S.; Li, J.; Niu, Z.; Zou, L.; Li, Y.; Yuan, J. Novel generation method of tooth surface points for variable transmission ratio gears. *Proceedings of the Institution of Mechanical Engineers Part C: Journal of Mechanical Engineering Science* **2022**, *236*, 5763-5782. https://doi.org/10.1177/09544062211062444

[17] Litvin, F.; Gonzalez-Perez, I.; Yukishima, K.; Fuentes, A.; Hayasaka, K. Generation of planar and helical elliptical gears by application of rack-cutter, hob, and shaper. *Computer Methods in Applied Mechanics and Engineering* **2007**, *196*, 4321-4336. https://doi.org/10.1016/j.cma.2007.05.003

[18] Han, X.; Zhang, X.; Zheng, F.; Man, X.; Jun, T. Mathematic model and tooth contact analysis of a new spiral non-circular bevel gear. *Journal of Central South University* **2022**, *29*, 157-172. https://doi.org/10.1007/s11771-022-4898-8

[19] Liu, D.; Lv, Z.; Li, B. Mathematical model and geometrical design method of noncircular face gear with intersecting axes. *Proceedings of the Institution of Mechanical Engineers, Part C: Journal of Mechanical Engineering Science* **2021**, *235*, 5902-5914. https://doi.org/10.1177/0954406221990708

[20] Zheng, F.; Chen, D.; Liu, Y. A generic algorithm of non-circular gear tooth profile. *Journal of Mechanical Transmission* **2013**, *37*, 64-66.

[21] Liu, Y.; Ning, S.; Hu, S.; Li, W. High**-**Order Non**-**Circular Helical Gear Designed Based on Conversion Method of Tooth Profile. *Modular Machine Tool & Automatic Manufacturing Technique* **2024**, *01*, 37-42.

[22] Han, J.; Li, D.; Tian, X.; Lian, X. Linkage model and interpolation analysis of helical non-circular gear hobbing. *Journal of the Brazilian Society of Mechanical Sciences and Engineering* **2020**, *42*, 582. https://doi.org/10.1007/s40430-020-02663-1

[23] Liu, Y.; Zhu, L. Research on non-circular helical gear NC hobbing linkage control scheme based on variable transmission ratio. *Proceedings of the Institution of Mechanical Engineers, Part B: Journal of Engineering Manufacture* **2022**, *236*, 1433-1442. https://doi.org/10.1177/09544054221076240

[24] Xu, H.; Shen, B. Noncircular planetary gear mechanism with double-arc pitch curve. *Journal of China Coal Society* **2010**, *35*, 691-695.

[25] Li, D.; Liu, Y.; Gong, J.; Wang, T. Design of a Noncircular Planetary Gear Mechanism for Hydraulic Motor. *Mathematical Problems in Engineering* **2021**, *2021*, 1-9. https://doi.org/10.1155/2021/5510521

Submitted: 01.4.2024

Accepted: 24.10.2024

Yongping Liu*
School of Mechanical and Electrical Engineering, Lanzhou University of Technology, Lanzhou, China;
State Wenzhou Engineering Institute of Pump and Valve, Lanzhou University of Technology, Wenzhou, China

Juan Wang
Changbin Dong
Fuqiang Wang
School of Mechanical and Electrical Engineering, Lanzhou University of Technology, Lanzhou, China

*Corresponding author:
cameliu@163.com